CFD Simulation of Flow around a Fixed Paired-Column Semi-Submersible

Weiwen Zhao*, Decheng Wan‡

State Key Laboratory of Ocean Engineering, School of Naval Architecture, Ocean and Civil Engineering, Shanghai Jiao Tong University, Collaborative Innovation Center for Advanced Ship and Deep-Sea Exploration, Shanghai 200240, China

*Presenting author: weiwen.zhao@sjtu.edu.cn

‡Corresponding author: dcwan@sjtu.edu.cn

Abstract

The Paired-Column Semi-Submersible (PC Semi) is a concept design by Houston Offshore Engineering (HOE). It distinguished from conventional semi-submersibles from three aspects: eight columns rather than four, rectangular columns rather than square and larger column slenderness. The current study numerically investigate the flow around a fixed PC-Semi at different velocities and current headings. The finite volume CFD solver naoe-FOAM-SJTU is utilized to archive all simulations. Turbulence flow around the semi-submersible is modeled by shear stress transport based delayed detached-eddy simulation (SST-DDES). The present computed drag forces are compared with existing experimental and numerical results. Instantaneous flow visualizations are presented and analyzed. This preliminary study show comprehensive wake interactions between columns and provide a better understanding of Vortex-Induced Motions (VIM) mechanism for multi-column offshore structures.

Keywords: multi-column; wake interference; current heading; naoe-FOAM-SJTU solver

Introduction

Flow past bluff bodies, such as chimneys, bridges, marine cables, risers and offshore platforms may induce flow separation and vortex shedding within a certain range of current speed. The periodic vortex shedding will cause oscillating hydrodynamic forces on bodies in transverse direction. For elastically mounted structures, transverse motions occur under the excitation of these fluctuation forces. The phenomena are commonly observed and gain much attention of engineers and scientists in the field of offshore engineering. It is termed vortex-induced vibrations (VIV) for marine cables and risers and vortex-induced motions (VIM) for large-volume offshore platforms. Despite a considerable number of experimental, numerical studies have been carried out to investigate the process on various kinds of offshore platforms (see for example [1–5]), it remain crucial to understand the flow mechanism behind VIM.

Model tests is the most common research method for VIM. Due to the high cost as well as speed limit of current generation in deepwater offshore basin, VIM model tests are usually conducted in towing tank or water circular channel. The model scale ratio from prototype is limited by the dimensions of towing tank and facilities. According to Fujarra et al. [6], small-scale tests with floating units subjected to VIM are generally employed due to the restriction of available facilities. The scale ratios for offshore platform VIM test vary from 40 to 100. Under such circumstances, it is impossible to ensure Reynolds number ($Re = U_C D / \nu$, where U_C is current velocity, D is characteristic length and ν is kinematic viscosity of fluid) equality between model and prototype. Typical Reynolds numbers for VIM model tests are in the order of 10^3 to 10^5, which fall into the sub-critical range. It is crucial to understand the flow characteristics around a fixed platform prior to an elastically mounted one in the sub-critical range.

Flow around single cylinder have been studied extensively in the past years. Delaney and Sorenson [7] experimentally investigated rounded-corner effect on the drag of an infinite length square cylinder with a wide range of Reynolds number (Re=10^4~2×10^6). However, the cylinder in their experiment was infinite. For cylinder with free end, Kawamura et al. [8]

measured surface pressure and Strouhal number around a finite circular cylinder on a flat plane at Re=3.2×10^4. The aspect ratio in their experiments varies from 1 to 8. Okamoto and Uemura [9] experimentally investigated the round-corner effects on aerodynamic forces and turbulent wake of a square column with free-end.

For flow past cylinder array, the wake interference between cylinders is important and has immediate significance in engineering applications. Sumner et al. [10] identified different flow patterns for flow past two cylinders in staggered arrangement with different center-to-center pitch ratios and angles of incidence by conducting experiments at sub-critical Reynolds number (Re=850 to 1900). Sayers [11] conducted experiments of flow past four equispaced cylinders at sub-critical Reynolds number (Re=3×10^4) with a varied staggered angle over the range of 0° to 180°. Liang et al. [12] experimentally and numerically studied flow around four rectangular columns with free end. The Reynolds number in their studies varies from 2.6 × 10^4 to 4.3 × 10^4.

In present study we numerically investigate the characteristics of flow around a fixed Paired-Column Semi-Submersible at different velocities and current headings. The detached-eddy simulation is employed for turbulence modeling. This paper is organized as follows: the geometry specifics of the semi-submersible are given first, followed by the introduction of computational domain, boundary conditions and mesh. Furthermore, the solver used in this study is briefly introduced. Then comes the computational results and discussions. Finally, some conclusions are drawn.

Methodologies

Geometry

This study is based on a Paired-Column Semi-Submersible (PC Semi) offshore platform, proposed and designed by the Houston Offshore Engineering (HOE), as shown in Figure 1. PC Semi is designed as an alternative to Spar platform for dry-tree application in the Gulf of Mexico (GoM). It can provide larger payload capability than Spar, while maintain the low dynamic response comparing with conventional semi-submersible. The overall height is 83.1m, in which the column height is 74.4 and pontoon height is 8.7m. The width of pontoon is 12.5m. The designed draft of the platform is 53.3m. PC Semi has eight rectangular columns rather than four squared columns compared with conventional semi-submersibles. The eight columns are divided into four outer columns (OC) and four inner columns (IC) with different dimensions. The OCs are connected to ICs with pontoons at four corner. The dimensions of OC and IC are 14.0m × 13.4m and 14.0m × 10.4m, respectively. The round corner radius for OC and IC are both 2.4m. The center-to-center distances of OC and IC are 96.0m and 50.3m, respectively. The aspect ratios (ratio between immersed length of the column and characteristic length) for OC and IC are 2.75 and 3.06, respectively.

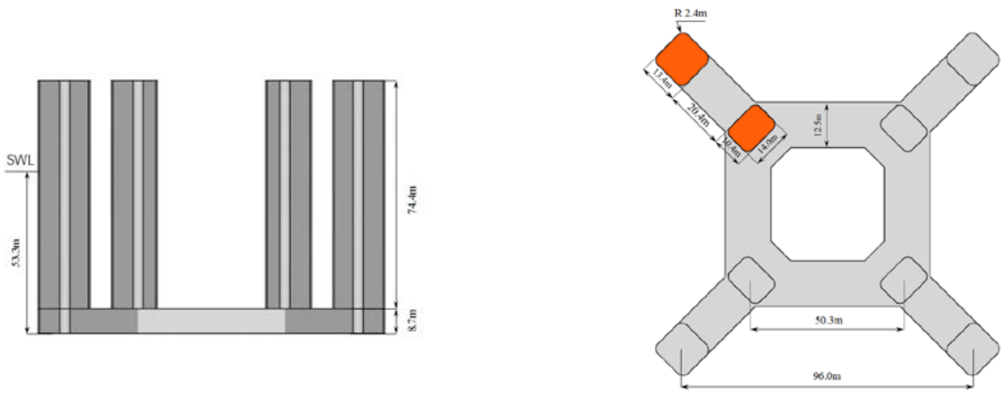

(a) Front view (b) Top view

Figure 1 Geometry of the PC Semi

Prior works to investigate VIM characteristics of the PC Semi have been presented as parts of the Research Partnership to Secure Energy for America (RPSEA) 4405 and 5404 projects. Meanwhile, a large number of experimental and numerical data have been published [13–18]. In these publications, the characteristic length (or effective diameter) of the rectangular column was defined as the diagonal length of the cross section without considering the corner radius. The characteristic lengths for OC and IC are 19.4m and 17.4m, respectively. In the present study, the model is scaled at ratio 1:54 which is the same with that in Antony's work [15].

Computational domain and boundary conditions

The model is displaced in a computational domain consisting of polyhedral cells. The computational domain is illustrated in Figure 2. This is a prior work of investigation for PC Semi VIM, which requires grids moving and deforming. Therefore the overset grids technique is utilized here. Two mesh blocks, namely the background grid and hull grid, are generated individually and then assembled into a single mesh. The domain of the background grid extends to $-14D \le x \le 28D$, $-11D \le y \le 11D$ and $-3H \le z \le 0$, where D is OC's characteristic length and H is the draft of PC Semi.

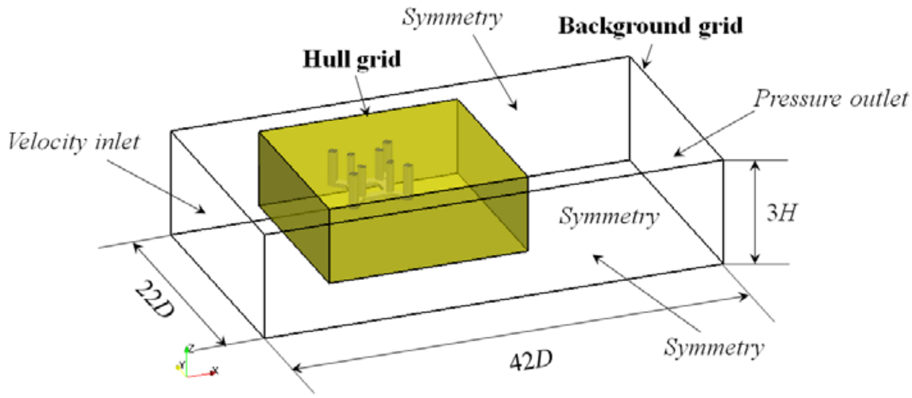

Figure 2 Computational domain and boundary condition

For background grid, Neumann boundary condition for velocity (fixed inlet) and Dirichlet boundary condition for pressure (zero gradient) were used on the upstream inlet patch ($x = -14D$), and vice versa for downstream outlet patch. Symmetry was applied for two sides and bottom of the domain. The free surface effect is neglected due to the small Froude number, thus the top plane at free surface is treated as symmetry. The boundary condition on hull surface is set to no-slip, i.e., zero for velocity and zero normal gradient for pressure.

Meshing strategy

Although the PC Semi in the current study is fixed, we use overset grid technique to perform our simulations as the present work will extends to VIM investigation which requires dynamic mesh. The overset grid approach is proved to be efficient and robust in the current solver [19]. As for stationary problems without grid moving, static overset mesh is applied. The domain connectivity information (DCI) just needed to be calculated only once at the beginning of the simulation. As mentioned before, the computational mesh consists of two mesh blocks, the background and hull grid which are generated individually. Figure 3 illustrates the static overset grid system in the current study. The background grid is hexahedral and has a uniform grid spacing. The hull grid is based on predominantly Cartesian cut cell approach and refined near hull and wake regions in order to capture the boundary layers and wake structures induced flow separations. Four different levels of refinement zones are utilized to archive higher accuracy in critical regions. In the vicinity of columns and pontoons, four prism cell layers are applied to hull boundary to capture the boundary layer development. For all cases, the non-dimensioned wall distance of the first layer satisfy $y+<5$ which make sure the first layer cells are located in the viscous sublayer.

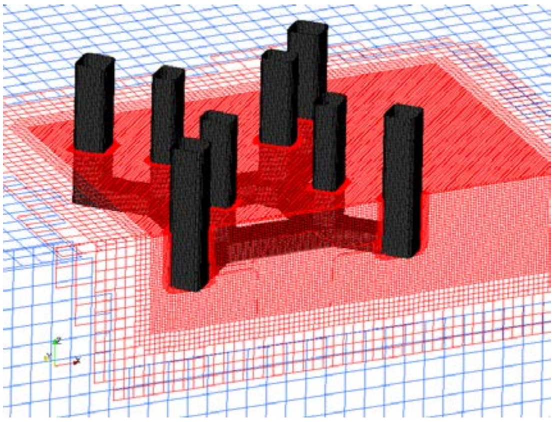

Figure 3 The overset grid distribution for 0° current heading (medium mesh)

Turbulence modeling

Flow past bluff bodies involves unsteady behavior and is dominated by large-scale structures. Therefore, it is not readily to solve these kinds of flow by statistical turbulence models. Essentially, large-eddy simulation (LES) is more suitable as it resolve the large-scale part of the turbulent eddies which has significant impact on the oscillating hydrodynamic forces of bodies. However, LES requires huge computational cost, most of which will be used to resolve the thin boundary layer when dealing with high Reynolds wall-bounded flows. According to Spalart [20], a pure LES simulation for practical engineering flow problem should be possible in approximately 2045. Detached-eddy simulation (DES) was proposed by Spalart [21] to address the challenge of massively separated flow at high Reynolds numbers. It combines the best practice of Reynolds-Averaged Navier-Stokes (RANS) and LES methods by employing unsteady RANS modeling in the near wall region and LES-like manner in the separated flow regions away from wall. In such a way, DES reduces grid resolution at boundary layer while maintaining the ability for accurately predicting eddy structures after flow separation. In the current study, naoe-FOAM-SJTU which is a solver developed based on OpenFOAM toolbox is utilized to perform all the simulations. We choose delayed DES (DDES) approach based on the two-equation Shear Stress Transport SST model for turbulence modeling [22].

Results and discussions

Two different current headings (0° and 22.5 °) are considered in our study. The definition of current heading herein are consistent with the model tests performed by Antony et al. [15], as shown in Figure 4.

Figure 4 Schematic of different current headings

Two different current velocities (U_c=2.0m/s, 2.75m/s) are investigated for each current heading. These velocities are for prototype and not scaled. For the 1:54 scaled model, the corresponding velocities are scaled by $1/\sqrt{54}$ and become 0.272m/s and 0.374m/s, respectively. The Reynolds number defined by OC's characteristic length ranges from 0.86 × 10^5 and 1.1 × 10^5.

The temporal derivatives are discretized using a second-order implicit backward differencing scheme. The convection term in momentum equation is discretized using a second-order upwind scheme, stabilized for transport (linear-upwind stabilized transport, LUST). For turbulent quantities, convection terms are discretized using a second-order TVD limited linear scheme. The merged PISO-SIMPLE (PIMPLE) algorithm is used for pressure-velocity decoupling.

Grid convergence study

Prior to all simulations, the accuracy and reliability of the current CFD approach is assessed by performing grid convergence study. The 0° and 0.272m/s case is selected to perform this study. Three different mesh sizes are considered. All simulations employs a time step of 0.02s. For overset grid system, grid refinement is performed for all mesh blocks. In this case, the background mesh block and the initial hexahedral mesh used generate hull mesh block by cut cell approach are refined by a factor of $\sqrt{2}$. Table 1 shows the results of grid convergence test. The mean drag parameter of numerical simulation are reasonably in good agreement with experiments, suggesting the present numerical simulations are accurate and reliable. The deviations of mean drag parameter $\overline{F_x}/(\rho U^2)$ and RMS lift parameter $F_y'/(\rho U^2)$ shows monotonic convergence, indicating the medium mesh is enough to resolve turbulent eddies around the hull. Therefore, the medium mesh is selected for all the remaining simulations.

Table 1 Results of grid convergence tests

Case	No. of cells			$\overline{F_x}/(\rho U^2)$ [m^2]	$F_y'/(\rho U^2)$ [m^2]
	Total	Background	Hull		
Coarse	1.04M	0.04M	1.00M	0.970	0.0644
Medium	2.53M	0.10M	2.43M	0.920	0.0303
Fine	6.25M	0.29M	5.96M	0.886	0.0280
Experiment[15]	-	-	-	0.912(±3.0%)	-

Forces and flow fields

Figure 5 shows the comparison of drag among the experimental and numerical results by Antony et al. [15] and present CFD results. Overall, all CFD methods agree well with experimental data, except AcuSolve and Fluent at 22.5° current heading. Fluent underestimated drag by 4.9% at 22.5° current heading and 0.374 m/s. However, no obvious deviations are observed in the present results.

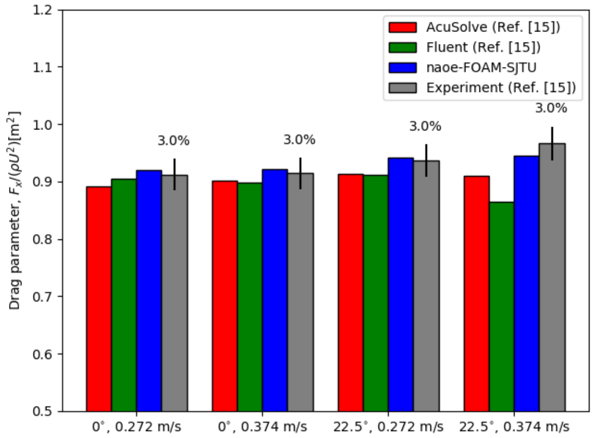

Figure 5 Comparison of drag between ref. [15] and present results

Figure 6 shows the instantaneous flow visualizations presented by streamwise velocity contours and streamlines on the cut-plane at z=-H/2 at U_c=0.272 m/s for different current headings. It can be seen that at 0° current heading, wake interference between side-by-side OCs is insignificant. However, the streamwise velocity increases between two upstream side-by-side ICs due to the narrower gap between ICs. Taking the upper-left OC as example, the streamlines behind it indicate there are two main recirculation bubbles located at position that has a lateral deviation to OC's x-direction centerline. The deviation is caused by the speed up flow between OC and corresponding IC. Looking from the streamwise direction, the wake interference between upstream and downstream OC is trivial because of the large spacing ratio L/D=4.95 (center-to-center distance to characteristic length). While the spacing ratio of ICs L/d=2.89 is small enough that the wake interference is non-trivial and cannot be neglected. Notably, the wakes of the downstream OCs are effected by ICs and are much wider due to the interaction between vortices of near wakes of the downstream OCs and upstream wakes. As for 22.5° current heading, a similar lateral deviation of recirculation region is observed behind the upstream OC. The staggered arrangement weakened the interaction between wakes of upstream and downstream ICs compared with 0° current heading. Nevertheless, the wake of downstream OC is influenced by the front IC and becomes wider.

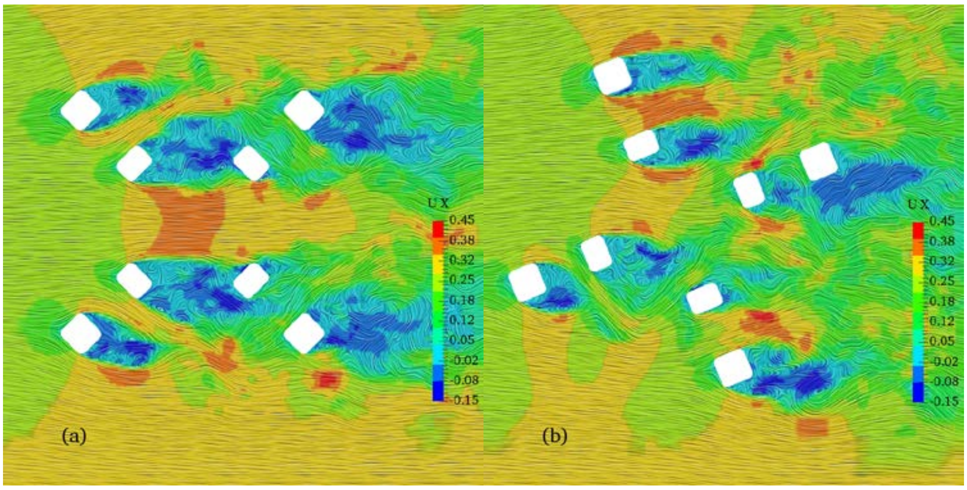

Figure 6 Instantaneous streamwise velocity contours and streamlines on the half-draft plane (z=-H/2) at U_c=0.272 m/s with (a) 0° and (b) 22.5°current headings

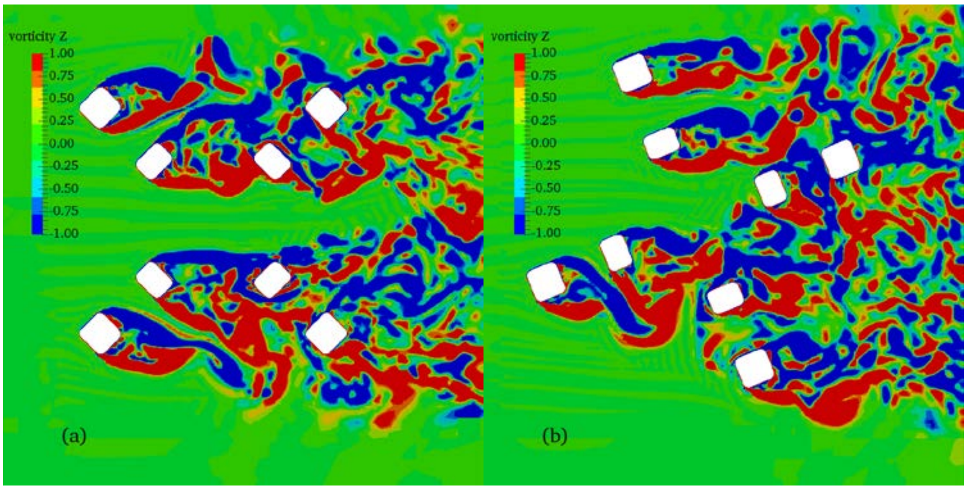

Figure 7 Instantaneous vorticity contours on the half-draft plane (*z*=-*H*/2) at U_c=0.272 m/s with (a) 0° and (b) 22.5°current headings

Figure 7 presents the instantaneous vorticity contour on the half-draft plane (*z*=-*H*/2) at U_c=0.272 m/s with different current headings. For upstream OCs and ICs at 0° current heading, the flow separation occurs in the vicinity of the rounded corner. No vorticities are found between the side-by-side ICs. The wakes of upstream ICs are strongly effected by upstream OCs, thus become much wider. In contrast, the upstream lateral IC at 22.5° current heading does not interfered by corresponding OC due to the providential orientation to current direction. Overall, the wakes of downstream columns interact with the vortices shed from upstream columns and break into small-scale eddies in the rear of PC Semi.

Figure 8 is the instantaneous pressure contour on the hull surface at U_c=0.272 m/s with different current headings. The view is seen from the upstream. For 0° current heading, the high-pressure region of the hull surface occurs exactly at the rounded-corner of the upstream OCs and ICs. For 22.5° current heading, it also appears at some downstream columns due to the staggered arrangement. It worth noting that in perpendicular surface to the high-pressure region for some columns, there exists some low-pressure regions which, in conjunction with the high-pressure regions, will result higher rotational moments around z-axis in compare with 0° current heading.

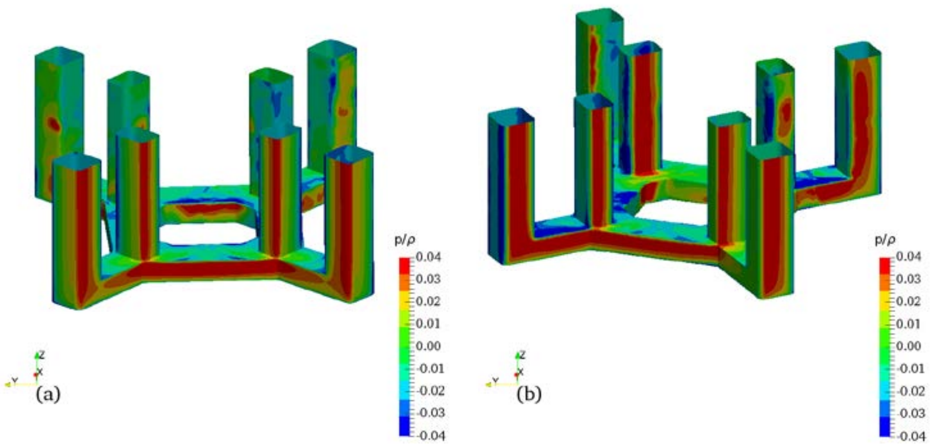

Figure 8 Instantaneous pressure contour on the hull surface at U_c=0.272 m/s with (a) 0° and (b) 22.5°current headings

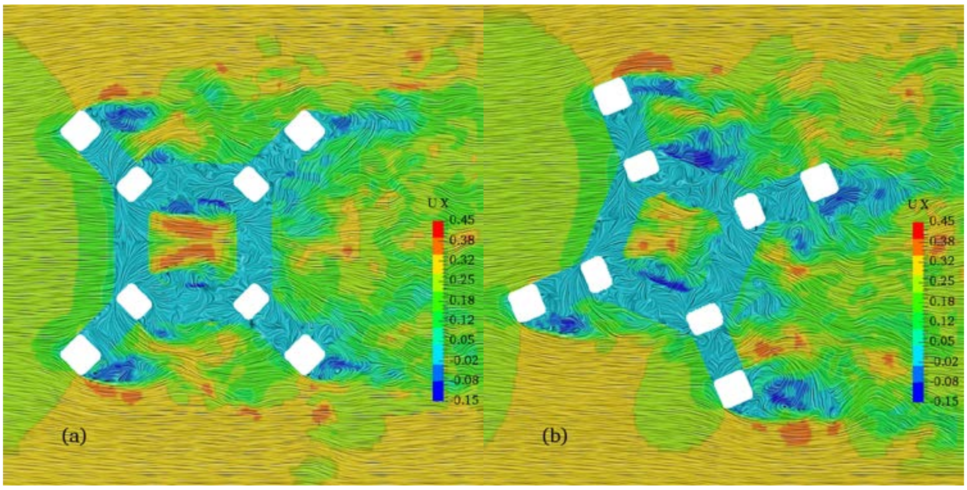

Figure 9 Instantaneous streamwise velocity contours and streamlines on the plane above pontoon at U_c=0.272 m/s with (a) 0° and (b) 22.5°current headings

Figure 9 presents the instantaneous streamwise velocity contours and streamlines on the plane above pontoon with different current headings. It clearly shows that the pontoon suppresses vortex sheds from the columns interior. In the region above moon pool, the high velocity area is smaller than that on the plane at $z=H/2$ in Figure 6. The diminution of streamwise velocity is induced by the large recirculation bubble around pontoon in the moon pool, as illustrated in Figure 10. Figure 10 also reveals that vortex mainly sheds from bottom shape corner of the pontoon. The vortex that sheds from top shape corner of the pontoon is mainly suppressed by the large flow velocities between upstream ICs.

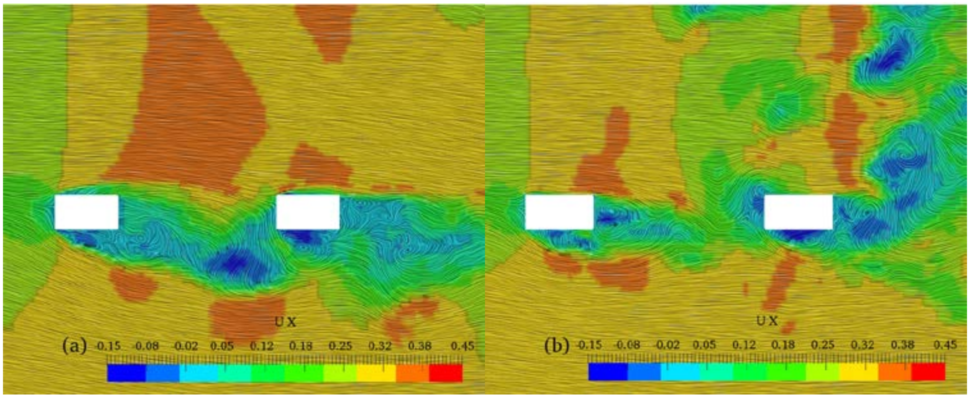

Figure 10 Instantaneous streamwise velocity contours and streamlines on the longitudinal section (y=0) at U_c=0.272 m/s with (a) 0° and (b) 22.5°current headings

Conclusions

In the present study, flow past a fixed Paired-Column Semi-Submersible at model scale 1:54 are numerically investigated at different flow velocities and current headings. The simulations are performed by the finite volume solver naoe-FOAM-SJTU developed on top of the OpenFOAM framework. The following conclusion can be drawn:

1. The drag parameters with 0° current heading vary little between current velocity 0.272m/s and 0.374m/s. However, they increase when the current heading changes from 0° to 22.5°. At 22.5° current heading, larger velocity will result in larger drag parameters.

2. Distinct wake interferences are observed at 0° current heading between ICs. Consequently, the pressures on the hull surface of downstream columns oscillate much stronger than that of upstream. At 22.5° current heading, surface pressure oscillations of downstream columns are much weaker due to the staggered arrangement of ICs.
3. Pontoons suppress vortex sheds from interior of the columns. Recirculation regions are observed in the moon pool behind the upstream pontoon.

The above conclusions can help us better understanding the wake interference in multi-column offshore structures. The current numerical approaches can be easily extended to VIM phenomena of the PC Semi. Investigations of the current headings effects on dynamic VIM response characteristics of PC Semi are ongoing.

Acknowledgements

This work is supported by the National Natural Science Foundation of China (51379125, 51490675, 11432009, 51579145), Chang Jiang Scholars Program (T2014099), Shanghai Excellent Academic Leaders Program (17XD1402300), Program for Professor of Special Appointment (Eastern Scholar) at Shanghai Institutions of Higher Learning (2013022), Innovative Special Project of Numerical Tank of Ministry of Industry and Information Technology of China (2016-23/09) and Lloyd's Register Foundation for doctoral student, to which the authors are most grateful.

References

[1] Finnigan, T., and Roddier, D. (2007) Spar VIM model tests at supercritical reynolds numbers, *Proceedings of the 26th International Conference on Offshore Mechanics and Arctic Engineering*, San Diego, California, USA, 3, 731–740.

[2] Roddier, D., Finnigan, T., and Liapis, S. (2009) Influence of the Reynolds number on spar Vortex Induced Motions (VIM): Multiple scale model test comparisons, *Proceedings of the ASME 28th International Conference on Ocean, Offshore and Arctic Engineering*, Honolulu, Hawaii, USA, 5, 797–806.

[3] Gonçalves, R.T., Fujarra, A.L.C., Rosetti, G.F., and Nishimoto, K. (2010) Mitigation of vortex-induced motion (VIM) on a monocolumn platform: Forces and movements, *Journal of Offshore Mechanics and Arctic Engineering* **132**(4), 041102.

[4] Waals, O.J., Phadke, A.C., and Bultema, S. (2007) Flow induced motions of multi column floaters, *Proceedings of the 26th International Conference on Offshore Mechanics and Arctic Engineering*, San Diego, California, USA, 1, 669–678.

[5] Gonçalves, R.T., Nishimoto, K., Rosetti, G.F., Fujarra, A.L.C., and Oliveira, A.C. (2011) Experimental study on vortex-induced motions (VIM) of a large-volume semi-submersible platform, *Proceedings of the ASME 2011 30th International Conference on Ocean, Offshore and Arctic Engineering*, Rotterdam, The Netherlands, 7, 1–9.

[6] Fujarra, A.L.C., Rosetti, G.F., De, W., and Gonçalves, R.T. (2012) State-of-art on Vortex-Induced Motion: A comprehensive survey after more than one decade of experimental investigation, *Proceedings of the ASME 2012 31st International Conference on Ocean, Offshore and Arctic Engineering*, 4, 561–582.

[7] Delany, N.K., and Sorensen, N.E. (1953) Low-speed Drag of Cylinders of Various Shapes, *National Advisory Committee for Aeronautics*.

[8] Kawamura, T., Hiwada, M., Hibino, T., Mabuchi, I., and Kumada, M. (1984) Flow around a Finite Circular Cylinder on a Flat Plate : Cylinder height greater than turbulent boundary layer thickness, *Bulletin of JSME* **27**(232), 2142–2151.

[9] Okamoto, S., and Uemura, N. (1991) Effect of rounding side-corners on aerodynamic forces and turbulent wake of a cube placed on a ground plane, *Experiments in Fluids* **11**(1), 58–64.

[10] Sumner, D., Price, S.J., and Païdoussis, M.P. (2000) Flow-pattern identification for two staggered circular cylinders in cross-flow, *Journal of Fluid Mechanics* **411**, 263–303.

[11] Sayers, A.T. (1988) Flow interference between four equispaced cylinders when subjected to a cross flow, *Journal of Wind Engineering and Industrial Aerodynamics* **31**(1), 9–28.

[12] Liang, Y., Tao, L., Xiao, L., and Liu, M. (2016) Experimental and Numerical Study on Flow Past Four Rectangular Columns in Diamond Configuration, V001T01A044.

[13] Zou, J., Poll, P., Roddier, D., Tom, N., and Peiffer, A. (2013) VIM testing of a paired column semi submersible, *Proceedings of the ASME 2013 32nd International Conference on Ocean, Offshore and Arctic Engineering*, Nantes, France, 7, V007T08A001.
[14] Antony, A., Vinayan, V., Halkyard, J., Kim, S.-J., Holmes, S., and Spernjak, D. (2015) A CFD based analysis of the Vortex Induced Motion of deep-draft semisubmersibles, *Proceedings of the Twenty-Fifth (2015) International Ocean and Polar Engineering Conference*, Kona, Big Island, Hawaii, USA, 1048–1055.
[15] Antony, A., Vinayan, V., Holmes, S., Spernjak, D., Kim, S.J., and Halkyard, J. (2015) VIM Study for Deep Draft Column Stabilized Floaters, *Offshore Technology Conference*, Houston, Texas, USA.
[16] Kim, S.J., Spernjak, D., Holmes, S., Vinayan, V., and Antony, A. (2015) Vortex-Induced Motion of Floating Structures: CFD Sensitivity Considerations of Turbulence Model and Mesh Refinement, *Proceedings of the ASME 2015 34th International Conference on Ocean, Offshore and Arctic Engineering*, St. John’s, Newfoundland, Canada, 2, V002T08A057.
[17] Vinayan, V., Antony, A., Halkyard, J., Kim, S.-J., Holmes, S., and Spernjak, D. (2015) Vortex-induced motion of deep-draft semisubmersibles: A CFD-based parametric study, *Proceedings of the ASME 2015 34th International Conference on Ocean, Offshore and Arctic Engineering*, St. John’s, Newfoundland, Canada, 2, V002T08A003.
[18] Kara, M., Kaufmann, J., Gordon, R., Sharma, P., and Lu, J. (2016) Application of CFD for Computing VIM of Floating Structures, *Offshore Technology Conference*, Houston, Texas, USA.
[19] Shen, Z., Wan, D., and Carrica, P.M. (2015) Dynamic overset grids in OpenFOAM with application to KCS self-propulsion and maneuvering, *Ocean Engineering* **108**, 287–306.
[20] Spalart, P.R. (2009) Detached-Eddy Simulation, *Annual Review of Fluid Mechanics* **41**(1), 181–202.
[21] Spalart, P., Jou, W., Strelets, M., and Allmaras, S. (1997) Comments on the feasibility of LES for wings, and on a hybrid RANS/LES approach, *Advances in DNS/LES* **1**, 4–8.
[22] Zhao, W., and Wan, D. (2016) Detached-Eddy Simulation of Flow Past Tandem Cylinders, *Applied Mathematics and Mechanics* **37**(12), 1272–1281.